Supplementary Figures and Movies

*****Figure and movie legend are included in a single PDF file (*i.e.*, SupplLegendFigures.pdf) with Supplementary Figures 1-5.

Suppl. Figure 1. Localizing and isolating punctate cellular structures. Image (A) is a segment (box in Fig. 3A) of image 1 of the TIRF image sequence shown in Suppl. Movie 1. Scale bar in (A) is 1 μm. The edges of punctate GLUT4 structures in (A) were first enhanced using a Differentiation of Gaussian (DOG) algorithm. The result of DOG processing (*i.e.*, image B) is an approximation of 2D-derivatization operation of (A). The edge of an object is defined as connecting pixels where the gradients of intensity variations are steepest. Thus, in a 2D-derivatization of the original image, the pixels on the edges will have intensity of 0. However, 2D-derivatization works well only with noise-free images. In contrast, DOG smoothes out noises first by convolving the original image (A) with two 2D-Gaussian functions with standard deviations of 1 and 2 pixels (100 nm per pixel) respectively. The difference (B) between these two smoothed images is the approximation of the 2D-derivatizative operation of the original image (A). Thus, in DOG processing, connecting pixels on edges have intensity close to 0 (5 in this case). Subsequently, a mask (binary image C) can be created in which pixels within the edges have uniform intensity of 1 and those outside have uniform intensity of 0. Applying (*i.e.*, multiple; red arrows) the mask to the original image (A) results in an image containing punctate GLUT4 structures (D). Individual GLUT4 structure is defined as a local intensity maximum, where the pixel intensity is higher or equal to those of all its eight immediate neighbors. Applying this rule to isolated regions containing punctate GLUT4 structures (D), a computer program automatically identifies all possible individual GLUT4 structures (red dots in E).

Suppl. Figure 2. Insulin increases a population of immobile GLUT4-containing structures in the TIRF evanescence field. Computation of corrected PC-values is described in Figure 3 legend and **Materials and methods**. Average PC-values and their associated standard errors of the mean were obtained from six individual adipocytes (A). For image clarity, only results for colocalization intervals (Δt) of 1s and 150s are shown (A). The corresponding average steady-state PC-values (see Fig. 3D) and their associated standard errors of the mean (from six cells) are plotted in (B) for the basal (squares) and insulin-stimulation (circles) conditions. Nonlinear least-square fitting (black and red lines in B) of these two sets of data were carried out using a two-exponential decay model (see equation in B), with the optimal fitting parameters and their associated fitting variances shown in the table below. As discussed in the **Results and discussion** section, the decay of steady-state PC-values over increasing Δt-intervals reveals dynamic properties of punctate GLUT4 structures imaged at 1 fps. These dynamic properties can be condensed into two exponential decay constants (T_1 & T_2) plus an immobile fraction (Y_0). Insulin stimulation increases the size of the immobile fraction by an average of ~10%. In addition, a fast (T_1=2-3s) and a slow (T_2=71-77s) dynamic components are also revealed, although their precise physical meanings are difficult to interpret at this stage. Nevertheless, T_1 could reflect lateral and vertical diffusion of punctate GLUT4 structures in the TIRF evanescence field, while T_2 could reflect 1) slower GLUT4 dynamics associated with clathrin-coated pits, 2) slow evolution of cellular structures near and on the coverslip-attached plasma membrane, and 3) slow drift in the TIRF images acquired over the 15 minutes experimental duration. Interestingly, neither T_1 nor T_2 is statistically different before and after insulin addition, which could be due to 1) the insulin-regulated changes in GLUT4 dynamics are insensitive to the time resolution at 1 fps, and/or 2) the percentage of GLUT4 vesicles in the TIRF evanescence

field undergoing insulin-regulated dynamic changes is too small. Amplitudes (A_1 and A_2) associated with T_1 and T_2 are both decreased upon insulin stimulation, but this is mostly because of a corresponding increase in Y_0 while the total decay amplitudes ($Y_0 + A_1 + A_2$) are relatively unchanged before and after insulin addition. In fact, the ratio A_1/A_2 is unchanged with insulin stimulation. Thus, at temporal resolution of 1 fps and using the temporal colocalization technique (Fig. 3), the only observable insulin effect on GLUT4 vesicular dynamics is a substantial increase of apparently immobilized GLUT4-containing structures in the TIRF evanescence field.

Suppl. Figure 3. Punctate GLUT4 structures colocalize with immobile clathrin-coated membranes in quiescent 3T3-L1 adipocyte. Using procedures demonstrated in Suppl. Figure 1, a pair of GLUT4 (A) and clathrin (D) images acquired under basal conditions (at the 0th min of the TIRF experiment) were converted into correspondent binary images containing only the punctate GLUT4 (B) and clathrin (E) structures. Scale bar in (B) is 5 μm. Similar processes were performed on all 600 pairs of GLUT4/clathrin images for the whole TIRF image sequence (*i.e.*, Suppl. Movies 3 & 4). Colocalization (yellow) of two binary clathrin images acquired under the basal conditions and separated by 1 minute shows most clathrin-coated pits have limited lateral mobility (F). Colocalization of the corresponding GLUT4 images also reveals some immobile punctate GLUT4 structures in the quiescent cell (C), which are mostly colocalized with the immobile clathrin-coated pits (*e.g.*, arrows in C & F).

Suppl. Figure 4. Insulin promotes GLUT4 accumulation in immobile clathrin-coated membranes. Day 7 differentiated adipocytes were co-transfected with clathrin-EGFP and

GLUT4-mRFP1, and two-color TIRF microscopy was carried out as described in **Materials and methods**. Using procedures demonstrated in Suppl. Figure 1, GLUT4 and clathrin images were converted into correspondent binary images containing only the punctate GLUT4 and clathrin structures. Representative colocalization images (yellow) between GLUT4 (red) and clathrin (green) structures before and 10 mins after insulin stimulation are shown in (A) and (B) respectively. Scale bar in (A) is 5 μm. Few colocalized GLUT4-clathrin compartments are found in the quiescent cell (A), which are noticeably increased 10 minutes after insulin stimulation (B). This is consistent with quantification (see Fig. 5 legend) of percentages of GLUT4 pixels colocalizing with clathrin pixels (red line in D) or verse vice (green line in D) for the whole TIRF image sequence (*i.e.*, Suppl. Movies 5 & 6). This ~10% increase in mutual GLUT4-clathrin colocalization after insulin stimulation (D) is consistent with the corresponding ~10% increase of immobile GLUT4-contaning structures revealed by temporal colocalization analysis shown in Suppl. Figure 2. Furthermore, temporal colocalization ($\Delta t = 2s$; see Fig. 3) of the GLUT4 (red line in C) and clathrin (green line in C) images reveals that the clathrin-coated pits are much less mobile than the punctate GLUT4 structures (*i.e.*, corrected PC-values of 65-75% for clathrin vs. 35-45% for GLUT4); see Suppl. Movie 6). Furthermore, insulin increases the degrees of temporal colocalization for GLUT4 structures while has little effect on the dynamics of the clathrin-coated pits (C). These results are consistent with visual inspection of the different dynamic properties associated with the GLUT4 and clathrin structures, and with the insulin-stimulated immobilization of a population of the GLUT4 structures in the TIRF evanescence field (see Suppl. Movies 5 and 6).

Suppl. Figure 5. Kinetics of single GLUT4 vesicle docking and fusion with the PM. This is another example of single GLUT4 vesicle docking and fusion, similar to the one described in Figure 6. However, this vesicle suddenly (within 0.1s) appears in the TIRF evanescence field and immediately docks to the PM (C).

*****All supplementary movies were encoded to be played by QuickTime Movie Player only. Except Movies 7 & 8, all movies were compressed using h264 algorithsm.

Suppl. Movie 1. Insulin stimulates GLUT4 exocytosis to the TIRF evanescence field. The TIRF experiment discussed in Figures 2 and 3 is shown in this movie. Images were acquired at 1 fps but encoded to be played at ~30 fps, with frame number (1 to 1200) shown in the bottom-left corner of each image. Insulin was added after the 300th image (*i.e.*, 5 minutes basal) with the room light turned on, resulting in bright and blurred images acquired in the next ~10s.

Suppl. Movie 2. Insulin promotes apparent immobilization of punctate GLUT4 structures in the TIRF evanescence field. The boxed region in Figure 3A is magnified and colocalization images (Δt = 1s) for the whole TIRF experiment (Suppl. Movie 1) are shown in this movie encoded to be played at 15 fps. Insulin was added at the 300th frame, and subsequent TIRF images were temporally brightened and blurred.

Suppl. Movie 3. Dynamic GLUT4 structures in the TIRF evanescence field. The two-color TIRF experiment discussed in Figures 4 and 5 is split into GLUT4-EGFP and clathrin-dsRed channels, producing two movies each containing 600 TIRF images acquired at 1 frame every two seconds. The first 150 images show GLUT4 dynamics under the basal conditions. Afterwards

insulin was added and subsequent TIRF images were temporally brightened and blurred. This movie is encoded to be played at 30 fps.

Suppl. Movie 4. Clathrin-coated pits have limited lateral mobility in the TIRF evanescence field. This is the clathrin-dsRed movie corresponds to the GLUT4-EGFP movie described in Suppl. Movie 3.

Suppl. Movie 5. Dynamic GLUT4 structures in the TIRF evanescence field. The two-color TIRF experiment discussed in Suppl. Figure 3 is split into GLUT4-mRFP1 and clathrin-EGFP channels, producing two movies each containing 600 TIRF images acquired at 1 frame every two seconds. The first 150 images show GLUT4 dynamics under the basal conditions. Afterwards insulin was added and subsequent TIRF images were temporally brightened and blurred. This movie is encoded to be play at 15 fps.

Suppl. Movie 6. Clathrin-coated pits have limited lateral mobility in the TIRF evanescence field. This is the clathrin-EGFP movie corresponds to the GLUT4-EGFP movie described in Suppl. Movie 5.

Suppl. Movies 7. A representative single GLUT4 vesicle fusion in an insulin-stimulated 3T3-L1 adipocyte. This movie shows the fusion event described in Figure 6, and is encoded to be played at real-time (*i.e.*, 10 fps). This movie is best viewed with a small view window on your movie player.

Suppl. Movies 8. A representative single GLUT4 vesicle fusion in a quiescent 3T3-L1 adipocyte. In the same adipocyte shown in Suppl. Movie 7, a single-vesicle fusion event was identified before insulin addition. Compared to that of the "after-insulin" fusion event shown in Suppl. Movie 7, the vesicle docking duration for this "before-insulin" fusion event is much longer. This movie is best viewed with a small view window on your movie player.

Suppl. Movie 9. Candidate fusion events identified by *Fusion Assistant*. A candidate fusion event is highlighted with a 1.3 × 1.3 μm red box centered at the peak vesicle intensity at the fusion time (T_F; see Fig. 7). This red box persists until *Fusion Assistant* loses tracking of the vesicle (*i.e.*, due to vesicle fusion or tracking difficulties; see **Materials and method**s). This movie shows all potential fusion events in 1 minute burst imaging at 10 fps (*i.e.*, the last minute of insulin stimulation; see illustration of the Burst protocol in Fig. 8) and was encoded to be played at the real time.

Suppl. Movie 10. Visually confirmed single-vesicle docking/fusion events. This movie shows the visually confirmed fusion events from candidate events presented in Suppl. Movie 9. The red boxes highlights the fusion process, while the preceding green boxes indicate the docked GLUT4 vesicles (see Fig. 7B). The movie is encoded to be played at the real time.

Supplementary Fig. 1; Huang *et al.* 2006

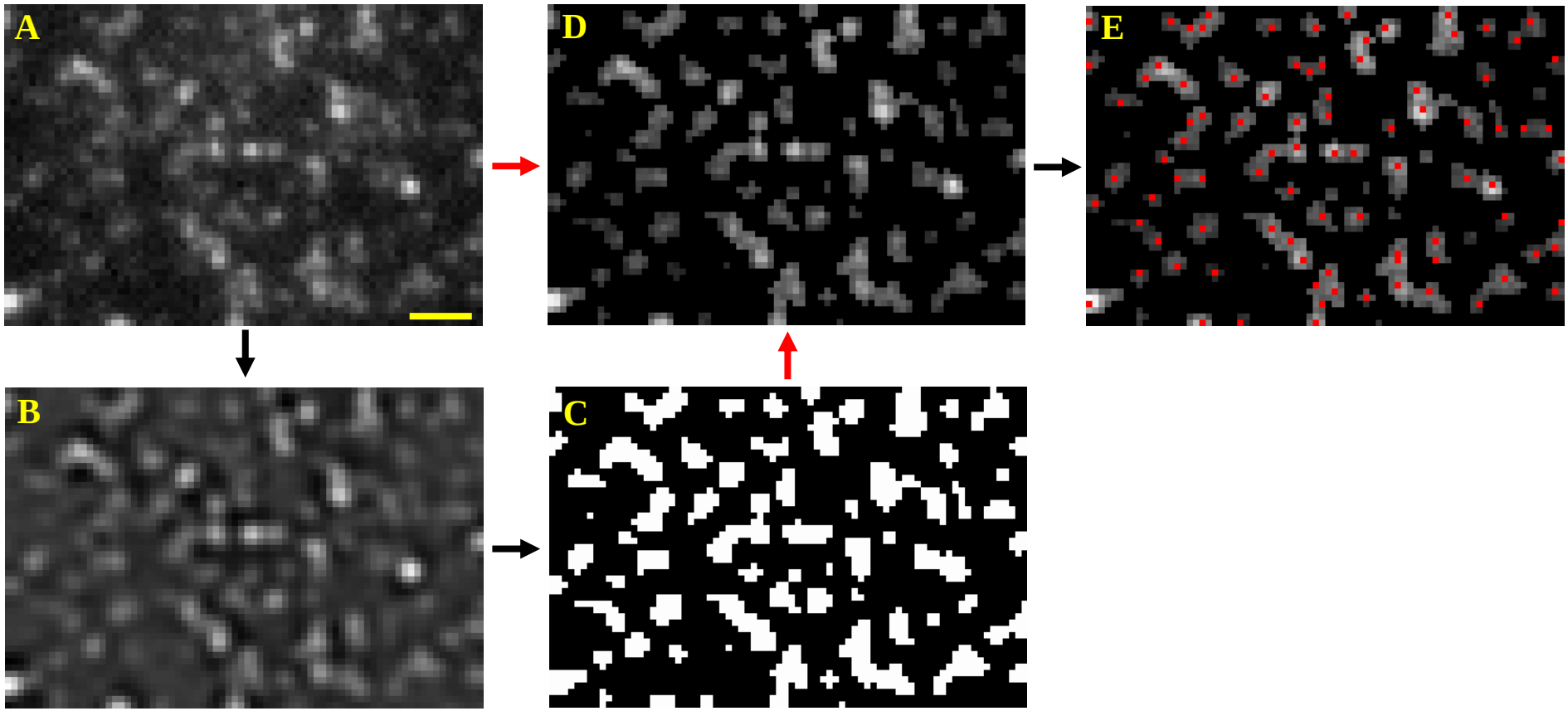

Supplementary Fig. 2; Huang *et al.* 2006

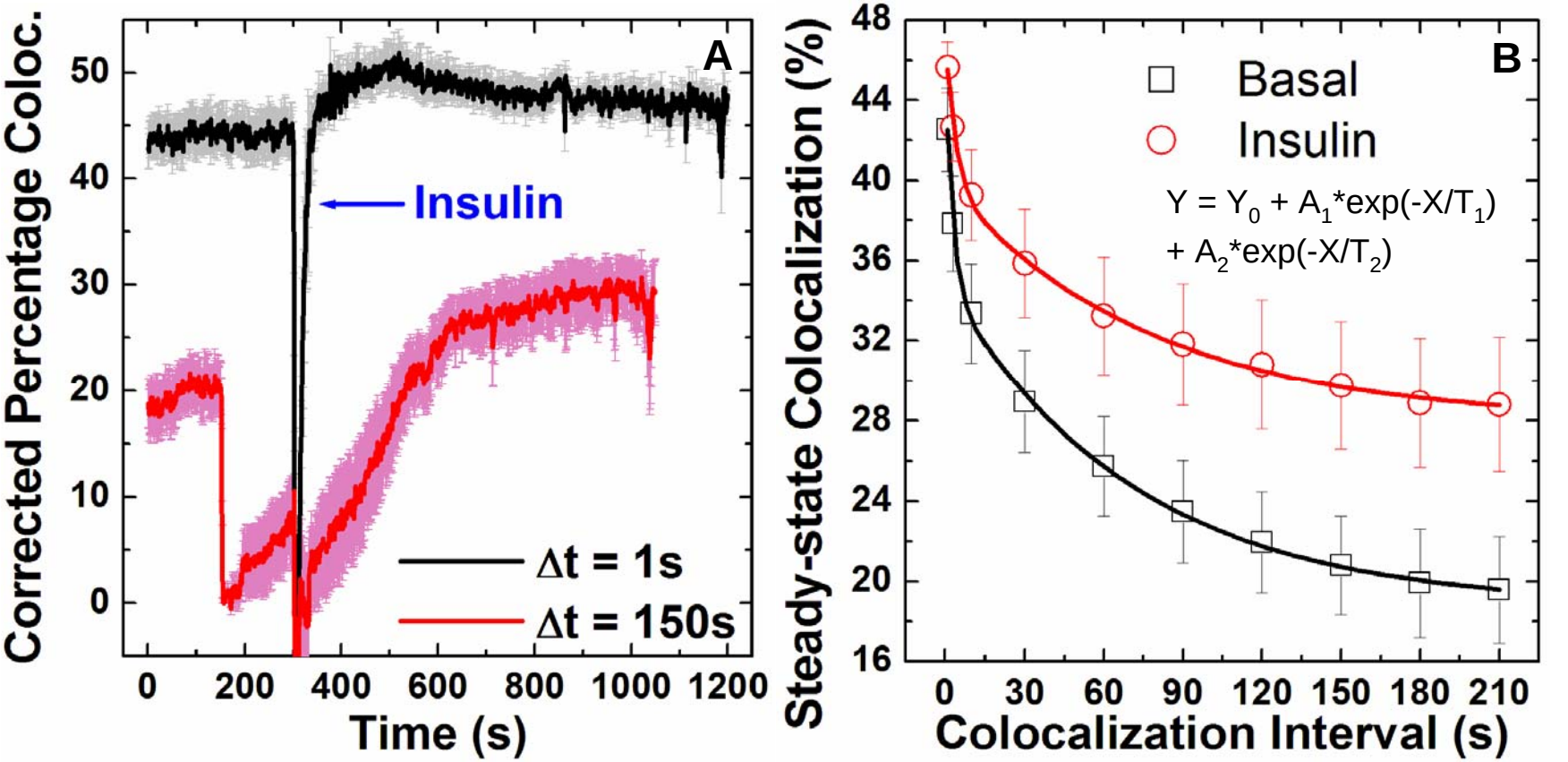

	Y_0	A_1	T_1(s)	A_2	T_2(s)	A_1/A_2
Basal	**18.8 ± 0.3**	**11.4 ± 0.7**	**2.7 ± 0.4**	**16.1 ± 0.4**	**71.4 ± 5.4**	**0.7 ± 0.1**
Insulin	**28.0 ± 0.5**	**7.6 ± 0.7**	**3.9 ± 0.9**	**11.8 ± 0.5**	**77.3 ± 10.6**	**0.6 ± 0.1**

Supplementary Fig. 3; Huang *et al.* 2006

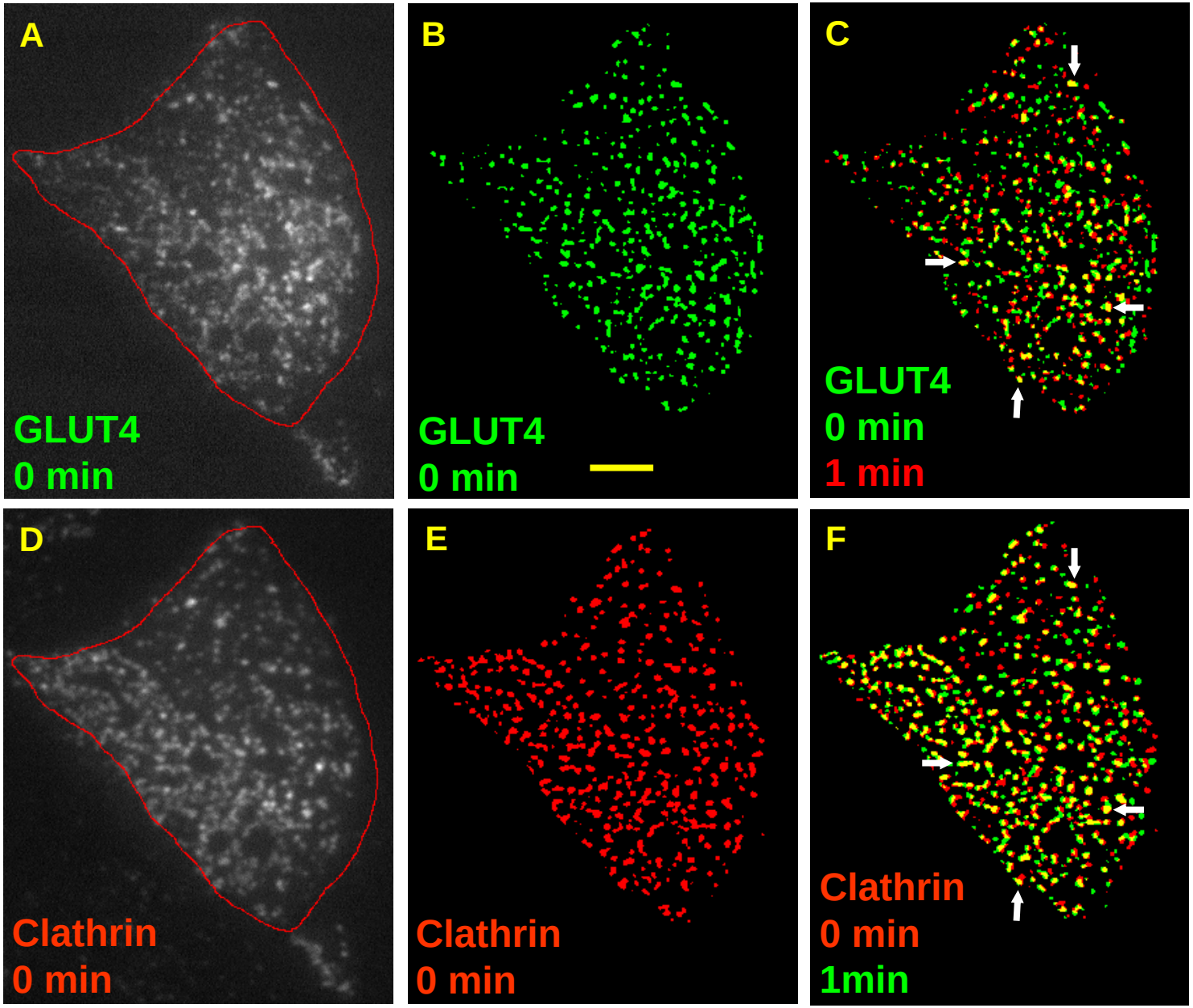

Supplementary Fig. 4; Huang *et al.* 2006

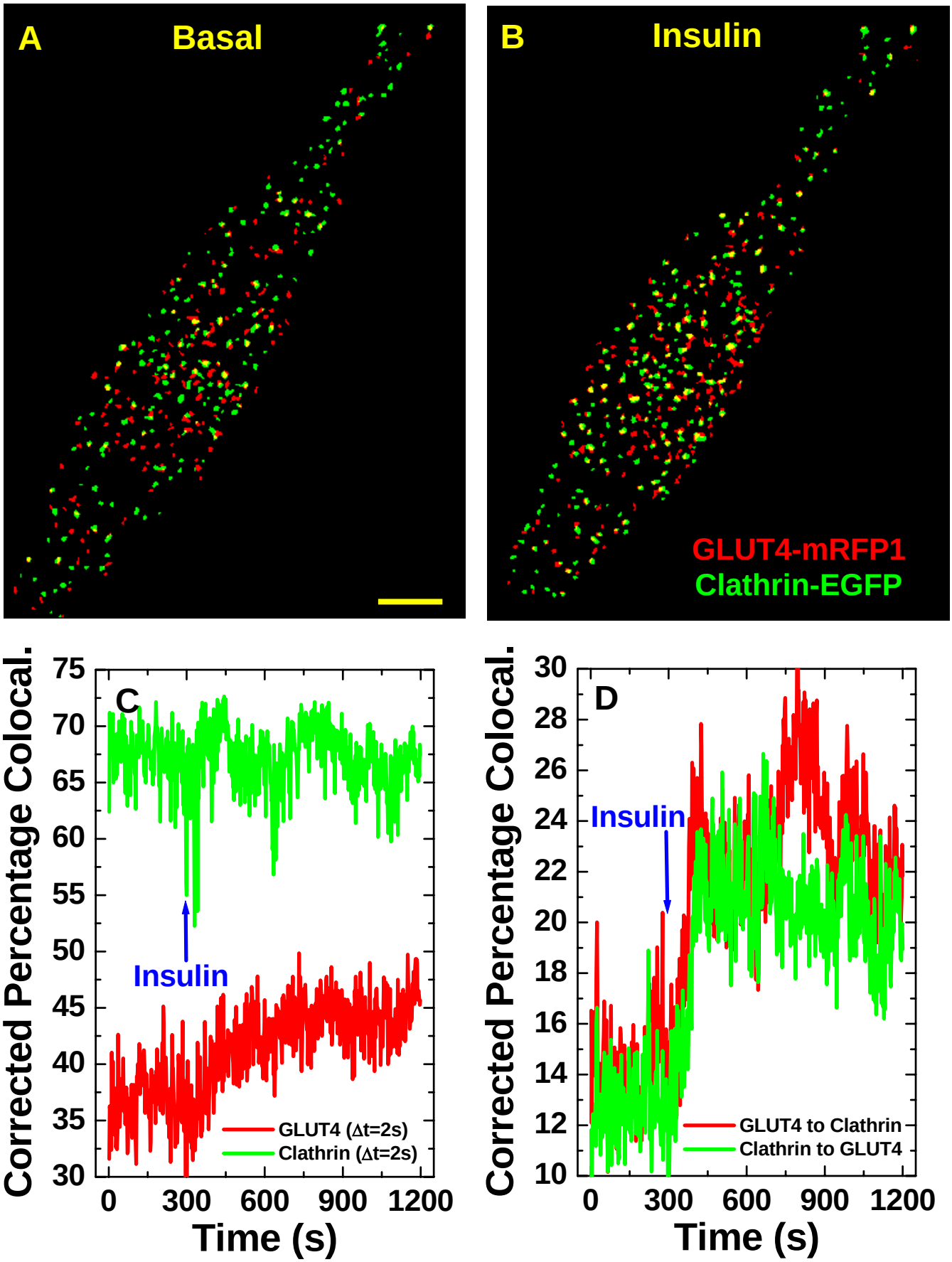

Supplementary Fig. 5; Huang *et al.* 2006